Fabrication of mid-infrared plasmonic antennas based on heavily doped germanium thin films

A. Samarelli, J. Frigerio, E. Sakat, L. Baldassarre, K. Gallacher, M. Finazzi, G. Isella, M. Ortolani, P. Biagioni, D.J. Paul

PII: S0040-6090(15)00978-5
DOI: doi: 10.1016/j.tsf.2015.10.005
Reference: TSF 34692

To appear in: *Thin Solid Films*

Received date: 22 April 2015
Revised date: 17 September 2015
Accepted date: 2 October 2015

Please cite this article as: A. Samarelli, J. Frigerio, E. Sakat, L. Baldassarre, K. Gallacher, M. Finazzi, G. Isella, M. Ortolani, P. Biagioni, D.J. Paul, Fabrication of mid-infrared plasmonic antennas based on heavily doped germanium thin films, *Thin Solid Films* (2015), doi: 10.1016/j.tsf.2015.10.005

Fabrication of mid-infrared plasmonic antennas based on heavily doped germanium thin films

A.Samarelli[1,*], J. Frigerio[2], E. Sakat[3], L. Baldassarre[4], K. Gallacher[1], M.Finazzi[3], G.Isella[2], M.Ortolani[5], P.Biagioni[3], D.J. Paul[1]

1. School of Engineering, University of Glasgow, Glasgow, G12 8LT, U.K.
2. L-NESS, Politecnico di Milano, Como, Italy.
3. Dipartimento di Fisica, Politecnico di Milano, Milano, Italy.
4. Center for Life NanoScience@Sapienza, Istituto Italiano di Tecnologia, Rome, Italy.
5. Physics Department, Sapienza University of Rome, Italy.

*** corresponding author: antonio.samarelli@glasgow.ac.uk**

Abstract - In this work, the growth and the fabrication of heavily doped germanium plasmonic antennas for mid-infrared applications is reported. By tuning the phosphorus doping concentration and the antenna geometrical parameters, plasma frequencies for targeting the 8-15 μm spectral region are achieved. 1 μm thick, heavily doped (2.3×10^{19} cm^{-3}) germanium was used to fabricate dipole antennas of 800 nm width with a gap spacing of 300 nm which demonstrate resonance frequencies around 13 μm and 13.5 μm for 2 μm and 3 μm long structures, respectively. This technology has the potential to be used for mid-infrared sensing applications of hazardous gases and liquids.

Keywords
Semiconductors, Germanium, Plasmonic, Mid-Infrared; Electron Beam; Etching, Antenna, Resonance

Introduction

Plasmonic devices foster the interaction of the light with matter. To date, surface plasmon polaritons and localized surface plasmons have been almost exclusively based on metals such as gold, aluminium and silver, which display plasma frequencies close to the visible and near infrared spectral regions. At these wavelengths, surface plasmons have demonstrated interesting properties to enable future communication architectures, high performance sensors and high resolution systems [1-6]. Of particular interest is the extension of these properties to other wavelength regions such as the mid-infrared (mid-IR) [7-11]. The reason behind this interest is that many molecules have molecular vibrational resonances providing spectral fingerprints in the spectral regions of 3 to 5 μm and 8 to 20 μm [1].

The availability of a material with plasmon resonances in this spectral region opens an extremely interesting research field for sensing bio-chemical analytes both in the liquid and gas phases. These devices could be exploited for gas detection, medical care and diagnostic as well as counter-terrorism detection of chemical and biological threats. One of the main challenges to enable mid-infrared plasmonics is related to the fundamental properties of the commonly used metals, which radically change their properties in this wavelength region of interest. The pursuit of different materials and geometries has suggested that highly doped semiconductor materials are a possible alternative to metals. The use of intrinsic silicon as a dielectric material for mid-IR photonics has already been proposed but the high losses at the longer wavelengths of interest make it not suitable for practical devices [12]. Germanium, on the contrary, is transparent over the entire mid-IR wavelength range and is compatible with CMOS (Complementary Metal Oxide Semiconductor) fabrication processes. When doped, Ge

has the further advantage over Si of a lower effective mass of conductivity for electrons ($m^* \approx 0.12$ for Ge compared to $m^* \approx 0.26$ for Si), which allows a higher plasma frequency to be reached for a given doping level. The plasma frequency is related to the effective mass of the free carriers (m^*) and the carrier density n, according to the relation $\omega_p \propto \sqrt{n/m^*}$. In addition, the possibility to control the carrier density and change the electrodynamic properties make doped semiconductors even more interesting for plasmonic applications as it is possible to fine tune the position of the plasma frequency over a wide spectral region [13].

Germanium film growth

1 μm Ge heterolayers were epitaxially grown by low-energy plasma-enhanced chemical vapour deposition (LEPECVD) [14,15] on a standard Si (001) wafer. The working principle of the LEPECVD reactor is reported in Fig. 1. The substrate wafer was exposed to a high intensity plasma, leading to growth rates of several nm/s through an efficient decomposition of the reactive molecules. High crystallinity and accurate control of the composition and the doping level [16] even in the presence of complex heterolayers [17,18] were obtained by a low-voltage arc discharge with ion energies in the range of tens of eV. The plasma source was connected to an ultra-high-vacuum chamber. The plasma profile was determined by a grounded anode in the lower part of the growth chamber and by a magnetic field, induced by a combination of coils and permanent magnets. The reactive gases SiH_4, GeH_4, PH_3 and B_2H_6, were fed into the growth chamber through a gas dispersal ring placed above the anode. The dopant gases were diluted in Ar at 1% and 5% respectively. The substrate was kept at a fixed potential with respect to the ground and the substrate temperature was adjusted between 200 °C and 750 °C by radiation heating. The deposition chamber had a base pressure of 10^{-7} Pa, whilst the working pressure was much higher, reaching 1 Pa. The growth rate was mainly

controlled by the plasma density and by the gas flow and it is weakly dependent on the substrate temperature. For this reason, the growth rate and the surface diffusivity of the atoms are completely decoupled and each can be individually optimized. Since the decomposition of the reactive molecules is dominated by the plasma, the surface chemistry between the substrate and the reactive molecules plays a small role in the determination of the alloy composition. Therefore the alloy composition can be easily controlled by the flow rates of the gases. The 1 μm thick germanium films investigated in this work were grown on p-type Si (001) substrates with a resistivity of 5-10 Ω·cm. No buffer layer was used between the silicon substrate and the Ge layer. Before the heteroepitaxy, the native oxide was removed by dipping the substrate in aqueous hydrofluoric acid solution. All samples were grown at 500 °C with a growth rate of ~ 1 nm/s and a GeH_4 flux of 20 sccm. The choice of a low temperature growth process and the absence of cyclic thermal annealing processes was used to avoid dopant out-diffusion and dopant clustering. The highest investigated active doping ($\sim 2.3 \times 10^{19}$ cm^{-3}), determined from 300 K Hall bar measurements on the same chip area and also through the Drude weight from mid-IR spectroscopy [13], was achieved by adding 0.15 sccm of PH_3 in-situ. A saturation of the activated doping level, as demonstrated in Fig. 2, is observed for flow rates above 0.15 sccm due to a delicate balanced process between the dopant incorporation and the dopant out diffusion during the growth. This is a common characteristic of many growth system such as molecular beam epitaxy and chemical vapour deposition [19].

Device fabrication

An aqueous solution of diluted hydrofluoric acid was used to remove the native oxide from the surface of the grown wafer. Neat hydrogen silsesquioxane (HSQ) electron-beam resist was spun at 3000 rpm and baked at 95 °C for 15 minutes on a hotplate to produce a final resist

layer thickness of 520 nm. A Vistec VB6 UHR electron-beam lithography tool was used to pattern the HSQ mask [20]. After exposure with a base dose of 1100 μC/cm^2 and a proximity error correction compensation, the samples were developed using a 25% tetramethylammonium hydroxide (TMAH) solution for 30 s followed by a rinse in deionized water for 60 s and a final dip for 15 s in propan-2-ol [21]. A Surface Technology System inductively coupled plasma tool was used to etch the antennas using a recipe of SF_6 and C_4F_8 in a mixed chemistry process. The ratio between the SF_6 and C_4F_8 was adjusted to obtain a balance between the etching and passivation gas processes. The process was optimised to obtain a vertical sidewall profile, minimum edge roughness and a reasonably fast etching time, which we reached with a flux of 30/90 sccm for SF_6/C_4F_8. The platen power was set to 12 W, the coil power to 600 W and the pressure was set to 1.6 Pa [22]. The etching process was assisted by a laser interferometer detection system to stop the process at the interface between the germanium and the silicon. The HSQ mask layer was finally removed in a diluted hydrofluoric acid etch to reduce the mid-infrared absorption of the HSQ layer. The final pattern, resulted in a dense array, with a coverage of 5 x 5 mm^2 of Ge antenna dipoles 1 μm deep etched, with lengths of 2 μm and 3 μm, a width of 800 nm and a gap of 300 nm.

Fig. 3 presents a scanning electron microscope (SEM) picture of part of the array, acquired with a Hitachi S4700 microscope with 10kV acceleration of the electrons. The optimised process resulted in an extremely high yield with more than 99% of the antenna present. The uniformity of the pattern and the final dimension of the fabricated devices were consistent over the entire area of the exposed pattern confirming good calibration of the proximity calibration and the absence of any loading effect in the etch process. The inset of Fig. 3, presents a 3 μm long antenna with a 300 nm gap length and Fig. 4, obtained by the slice-and-view technique in a dual ion- and electron-beam apparatus, demonstrates the good verticality of the optimized etching recipe.

Antenna Characterisation

The mid-IR response of materials for two different levels of doping in the 10^{17}-10^{19} cm^{-3} range has been characterised by Fourier-transform infrared spectroscopy (FTIR) based on a Michelson interferometer (Bruker IFS66v) [23]. A broadband glow bar mid-IR source was used to illuminate the sample under analysis and the signal was collected with a HgCdTe detector (MCT). The light was polarized with a with a wire-grid lithographic polariser on a KRS-5 substrate (by Specac). The angle of incidence was quasi-normal (12 degrees). We determined the transmittance spectra of the antenna array by dividing the spectral intensity transmitted through the area of the chip where antennas were present by a different area of the chip where the entire Ge film was etched away. In this way we could eliminate any contribution coming from impurity state absorption in the Si substrate. The transmittance spectra in the mid-IR range of the antenna arrays between 8 and 20 μm wavelength are reported in Fig. 5 and Fig. 6. In the following, we identify two different polarizations called co-polarisation and cross-polarisation, where the field is aligned along or across the antenna arm direction, respectively. The experimental results obtained clearly display a resonance peak in the 12-13 μm range for the highly doped Ge antennas array, which is characterized by a screened plasma frequency around 1000 cm^{-1}. Electromagnetic simulations are in fair agreement with the experiments and reveal that the observed resonance is associated to a longitudinal mode propagating inside the Ge antenna with hot-spots located at the Ge-air interface. The presence of this resonance peak appears only for the co-polarized spectrum of the dipole antenna with high doping (blue continuous line). Lastly, it is interesting to see that a slight shift of the resonance frequency (Fig. 6) is present for dipole antenna of two different lengths (2 μm and 3 μm). The sharp spectral feature around 16 μm that can be observed in all

spectra is due to the Raman-active Si phonon, which couples to IR light because of defects in the Si substrate. The tuning of the antennas with different gap sizes and antenna lengths will be analysed in future experiments.

Conclusions

We have analysed the spectral response of heavily doped Ge antennas working in the mid-infrared region. Both 2 μm and 3 μm long antennas with 300 nm gap spacings display plasma resonances in the spectral region between 8 μm to 13 μm where molecular absorption lines of glucose, DNA as well as hazardous liquid and gases are located. Since the effective mass of n-type Ge is $m^* = 0.12\ m_e$ the future aim is to further increase the level of the activated dopant to target the 3-5 μm spectral region where molecular absorption of gases such as CO, CO_2, CH_4 and N_2O are located. We believe that this research in exploiting Ge as a material for mid-IR plasmonic devices could have a substantial impact in creating integrated, low-cost, sensing devices with applications in environmental, healthcare and security monitoring.

Acknowledgments

The research leading to these results received funding from the European Union's Seventh Framework Programme under grant agreement n°613055. The authors would like to thank the staff of the James Watt Nanofabrication Centre at the University of Glasgow for help in the fabrication of the devices.

References

[1] E. Ozbay, Plasmonics: merging photonics and electronics at nanoscale dimensions, Science 311 (2006) 189–193.

[2] P. Biagioni, J.S. Huang, B. Hecht, Nanoantennas for visible and infrared radiation, Rep. Prog. Phys. 75 (2012) 024402.

[3] V. Giannini, A.I. Fernández-Domínguez, S.C. Heck,S.A. Maier, Plasmonic nanoantennas: fundamentals and their use in controlling the radiative properties of nanoemitters, Chem. Rev. 111 (2011) 3888-3912.

[4] S. Lal, S. Link, N.J. Halas, Nano-optics from sensing to waveguiding, Nature Photon. 1 (2007) 641-648.

[5] L. Novotny,N. van Hulst, Antennas for light, Nature Photon. 5 (2011) 83-90.

[6] R. Zia, J.A. Schuller, A. Chandran, M.L. Brnogersma, Plasmonics: the next chip-scale technology, Materials Today 9 (2006) 20-27.

[7] F. Neubrech, A. Pucci, Th.W.Cornelius, S. Karim, A. García-Etxarri, J. Aizpurua, Resonant plasmonic vibrational coupling in tailored nanoantenna for infrared detection, Phys. Rev. Lett. 101 (2008) 157403.

[8] R. Adato, A. Artar, S. Erramilli, H. Altug, Engineered absorption enhancement and induced transparency in coupled molecular and plasmonic resonator systems, Nano Lett. 13 (2013) 2584-2591.

[9] R. Adato, A.A. Yanika, J.J. Amsdenc, D.L. Kaplanc, F.G. Omenettoc, M.K. Honge, S. Erramilli and H.Altug, Ultra-sensitive vibrational spectroscopy of protein monolayers with plasmonic nanoantenna arrays, Proc. Natl. Acad. Sci. 106 (2009) 19227-19232.

[10] O. Limaj, S. Lupi, F. Mattioli, R. Leoni, M. Ortolani, M., Midinfrared surface plasmon sensor based on a substrateless metal mesh, Appl. Phys. Lett. 98 (2011) 091902.

[11] M. Schnell, P. Alonso-González, L. Arzubiaga, F. Casanova, L.El Hueso, A. Chuvilin, R. Hillenbrand, Nanofocusing of mid-infrared energy with tapered transmission lines, Nature Photon. 5 (2011) 283-287.

[12] R. Soref, Mid-infrared photonics in silicon and germanium, Nature Photonics 4 (2010)495-497.

[13] L. Baldassarre, E. Calandrini, A. Samarelli, K. Gallacher, D.J. Paul, J. Frigerio, G. Isella, E. Sakat, M. Finazzi, P. Biagioni, M. Ortolani, Mid-Infrared plasmonic platform based on heavily doped epitaxial Ge-on-Si: retrieving the optical constants of thin Ge epilayers in 39th Proc. Int. Conf. Infrared, Millimeter, THz Waves, Tucson, USA (2014) pp. 1-3.

[14] G. Isella, D. Chrastina, B. Rossner, T. Hackbarth, H.-J. Herzog, U. Konig, H. von Kanel, Low-energy plasma-enhanced chemical vapor deposition for strained Si and Ge heterostructures and devices, Solid State Electron. 48 (2004) 1317.

[15] C. Rosenblad, H. R. Deller, A. Dommann, T. Meyer, P. Schroeter, and H. von Kanel, Silicon epitaxy by low-energy plasma enhanced chemical vapor deposition, J. Vac. Sci. Technol. A 16 (1998) 2785-2780.

[16] S. Cecchi, T. Etzelstorfer, E. Müller, D. Chrastina, G. Isella, J. Stangl, A. Samarelli, L. Ferre Llin, D.J. Paul, Ge/SiGe superlattices for thermoelectric energy conversion devices, J. Mat. Sci. 48 (2013) 2829-2835.

[17] A. Samarelli, L. Ferre Llin, S. Cecchi, J. Frigerio, T. Etzelstorfer, E. Müller, Y. Zhang, J. R. Watling, D. Chrastina, G. Isella, J. Stangl, J. P. Hague, J. M. R. Weaver, P. Dobson, D. J. Paul, The thermoelectric properties of Ge/SiGe modulation doped superlattices, J. Appl. Phys. 113 (2013) 233704.

[18] L. Ferre Llin, A. Samarelli, S. Cecchi, T. Etzelstorfer, E. Müller Gubler, D. Chrastina, G. Isella, J. Stangl, J. M. R. Weaver, P. S. Dobson, D. J. Paul, The cross-plane thermoelectric properties of p-Ge/Si0.5Ge0.5 superlattices, Appl. Phys. Lett. 103 (2013) 143507.

[19] R. Camacho-Aguilera, Y. Cai, J. Bessette, L. Kimerling, J. Michel, High active carrier concentration in n-type, thin film Ge using delta-doping, Opt. Mater. Exp. 2 (2012)1462-1469.

[20] A. Samarelli, D.S. Macintyre, M.J. Strain, R.M. De La Rue, M. Sorel, S. Thoms, Optical characterization of a hydrogen silsesquioxane lithography process , J. Vac. Sci. Technol. B, 26 (2008)2290-2294.

[21] A. Samarelli, R.M. De La Rue, M. Sorel A. Canciamilla, F. Morichetti, A. Melloni, Precise fabrication of coupled ring-resonator structures, in Proc. European Conf. on Lasers Electro-Optics 2009 European Quantum Electron. Conf. CLEO Europe - EQEC 2009., pp.1,1, (009)

[22] M. Mirza, H. Zhou, X. Li, P. Velha, K. Docherty, A. Samarelli, G. Ternent, D.J. Paul, Nanofabrication of high aspect ratio (~50:1) sub-10 nm silicon nanowires using plasma etch technologies, J. Vac. Sci. Technol. B 30 (2012) 06FF02-1.

[23] P.R. Griffiths, J.A. de Haseth, Fourier Transform Infrared Spectrometry, Wiley: New York, 2007.

Fig. 1: A schematic diagram of the LEPECVD machine used for epitaxial growth.

Fig. 2: The measured calibrated active carrier concentration versus the phosphine (PH3) flux rate obtained from the growth system.

Fig. 3: An image of an angled view of one of the fabricated antenna arrays. In the inset a detailed view of one of the antennas with a gap of 300 nm and a length of each dipole arm of 3 μm is displayed.

Fig. 4: A cross section of one of the fabricated antennas obtained by the slice-and-view technique in a dual ion- and electron-beam tool. The substrate is first coated with a Pt layer and then Ga ions are used to cut the material.

This is used to demonstrate the good verticality of the etch profile.

Fig. 5: FTIR transmission measurements for the 3 μm dipole antennas patterned in highly doped and intrinsic material along with the measurements of the two different polarizations.

Fig. 6: FTIR transmission measurements are displayed for 2 μm and 3 μm dipole antennas with co-polarisation. A slight shift of the resonance peak is evident in the plot.

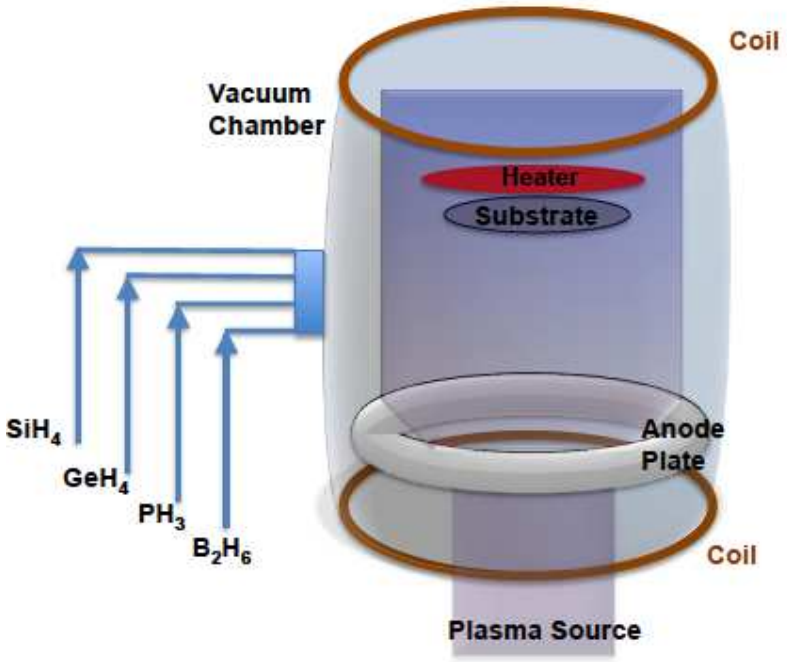

Figure 1

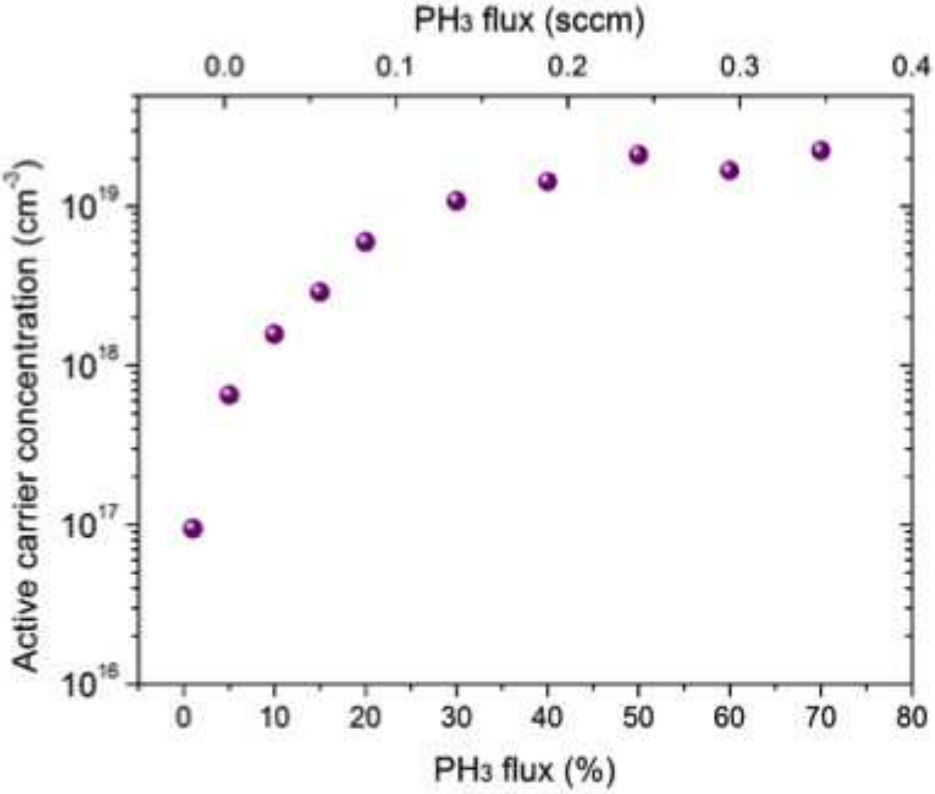

Figure 2

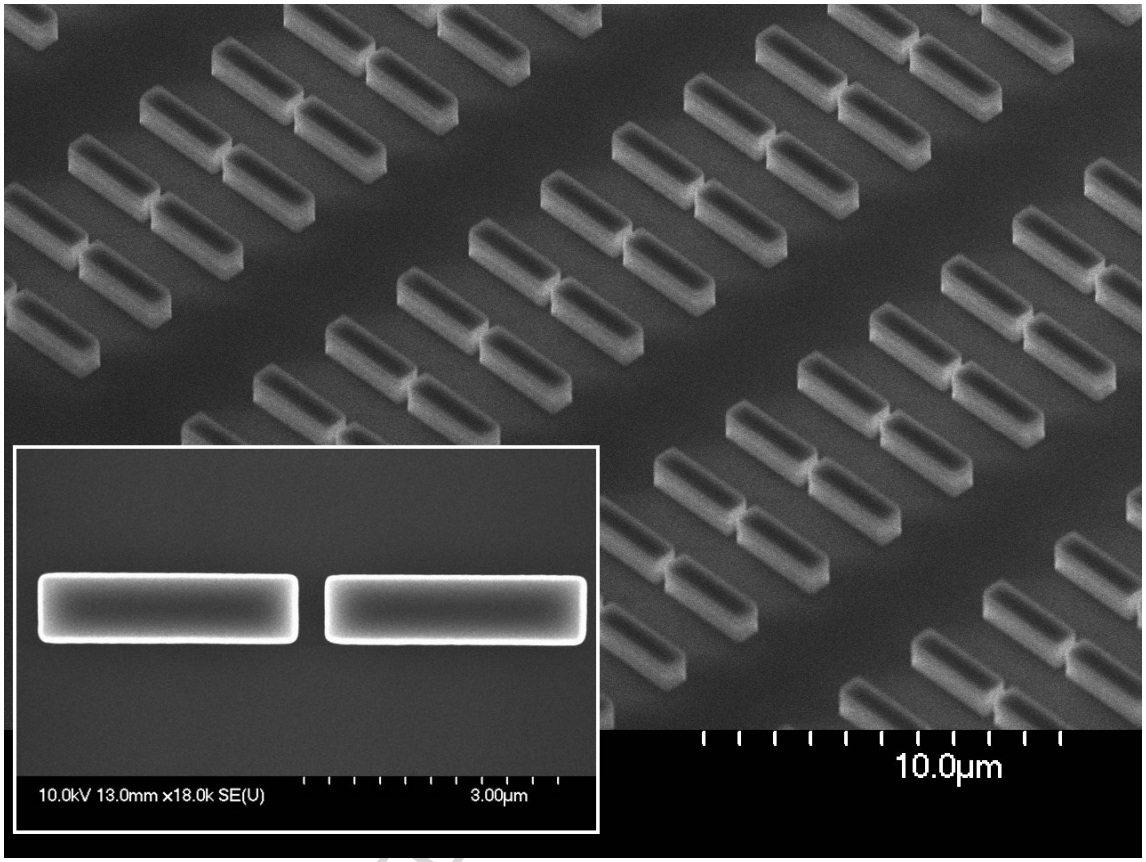

Figure 3

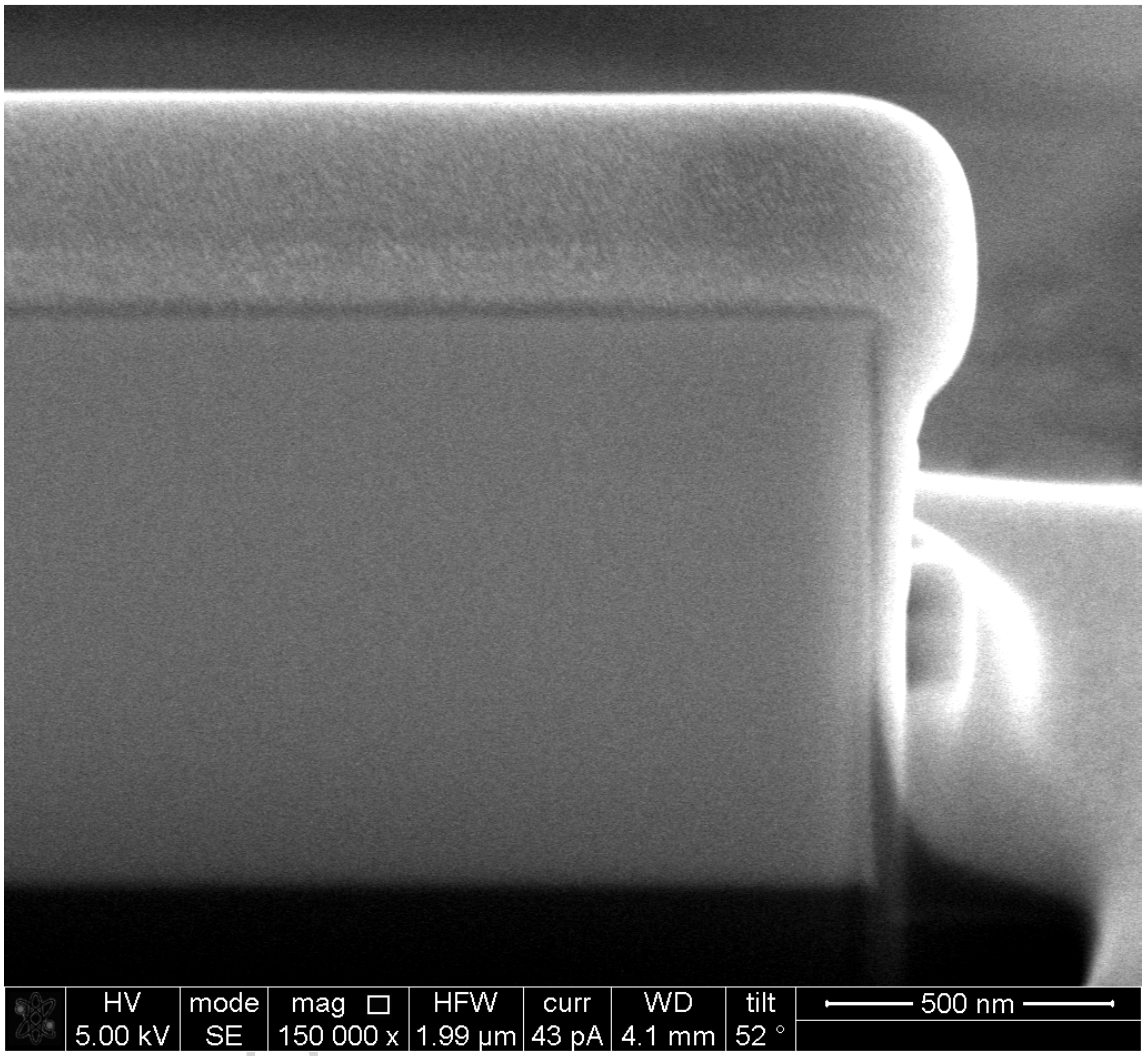

Figure 4

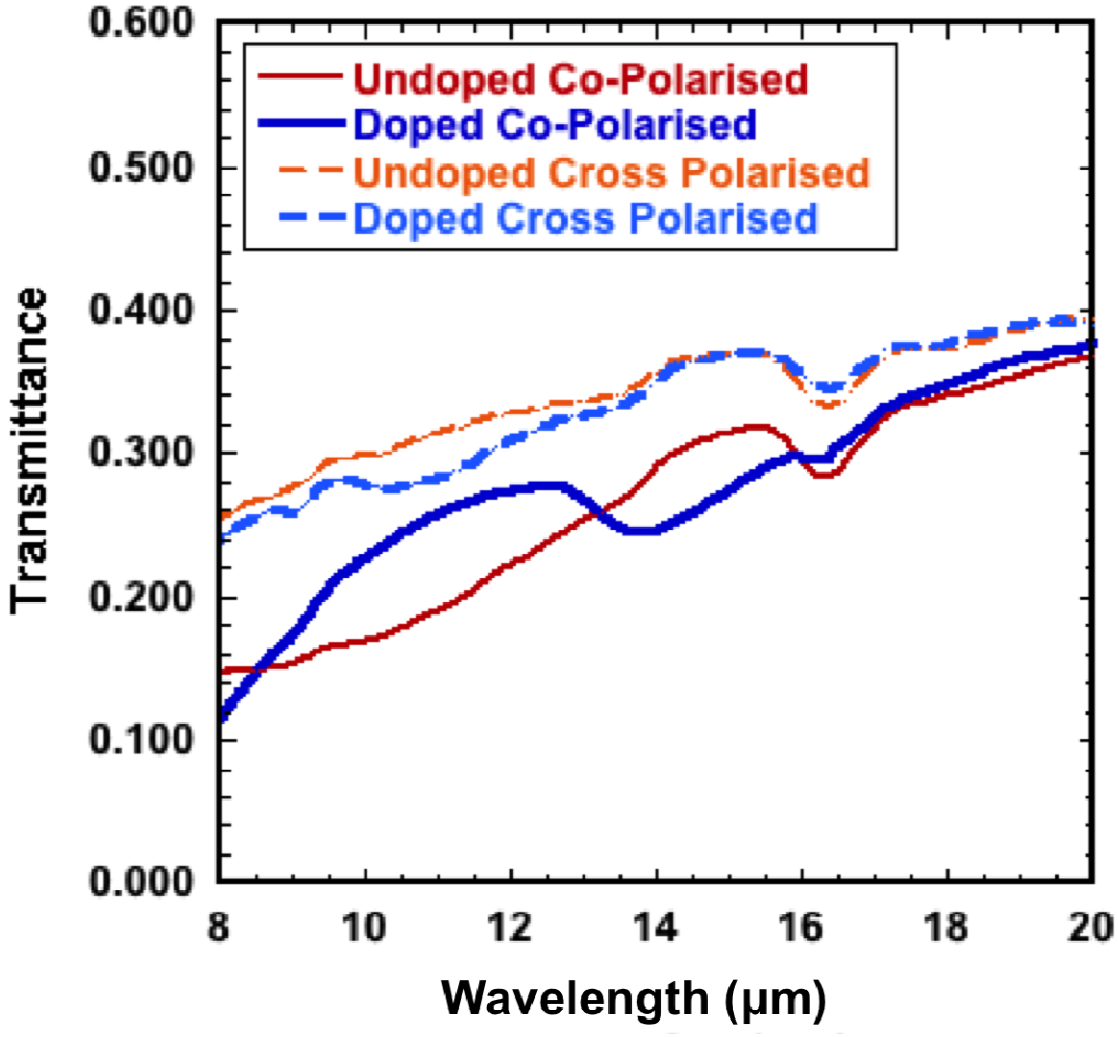

Figure 5

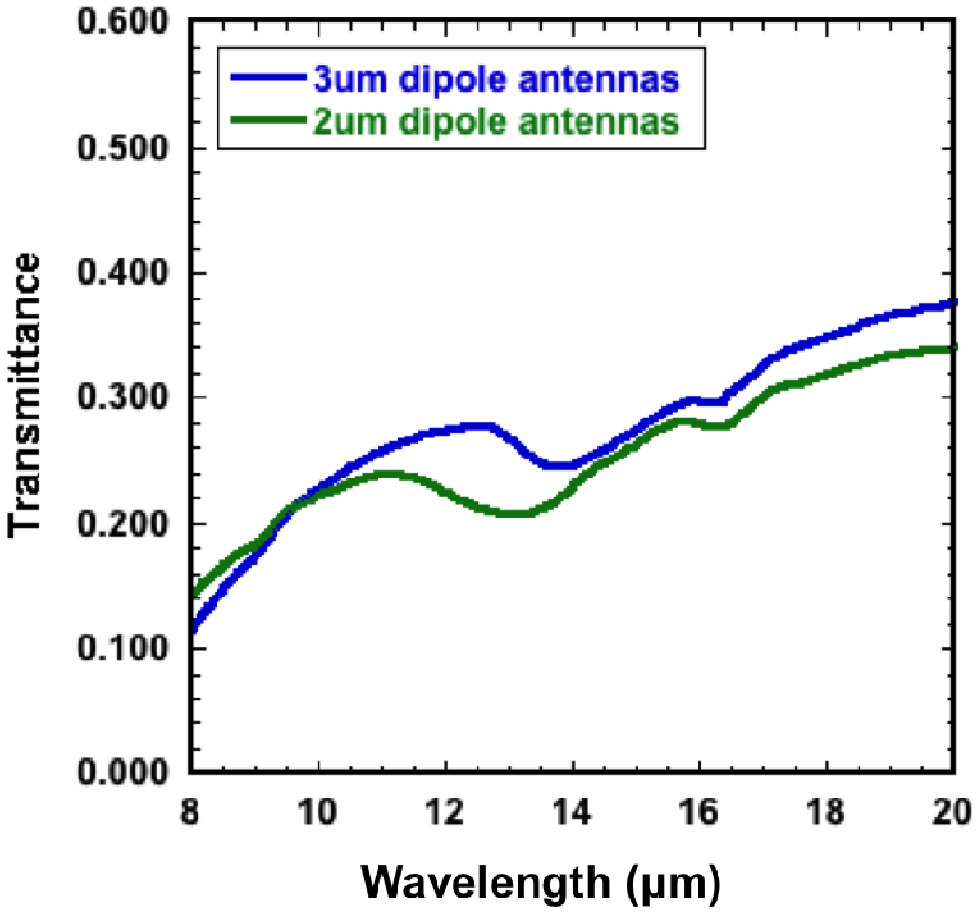

Figure 6

Highlights

- Germanium growth by low-energy plasma-enhanced chemical vapour deposition
- Detailed description of the germanium plasmonic dipole antennas fabrication process
- The mid-infrared spectral response of the plasmonic dipole antennas